Rubidium and Cesium Excitation Transfer in Nearly Adiabatic Collisions with Inert Gases *

Alan Gallagher
Joint Institute for Laboratory Astrophysics,†
Boulder, Colorado
(Received 19 January 1968)

The cross sections for rubidium $5^2P_{1/2} \rightleftarrows 5^2P_{3/2}$ and cesium $6^2P_{1/2} \rightleftarrows 6^2P_{3/2}$ excitation transfer due to inert-gas collisions have been measured. The temperature of the collision vessel has been varied from 300°K to 900°K in order to partially establish the velocity dependence of these cross sections (the alkali resonance-line optical depths were always much less than 1). The various cross sections exhibit a systematic behavior that can be combined to find the general shape of a "universal" cross section that ranges across six orders of magnitude, starting just below the threshold for "sudden" collisions. The surprisingly large influence of optical line broadening on these excitation-transfer measurements has been removed as a source of error.

INTRODUCTION

Collisional transfer of excitation between the fine-structure states of the lowest alkali-metal p doublets can easily be detected, and there is a long history of such measurements.[1] The standard technique is to excite an alkali metal to the ^2p_J state with one "D line" of the resonance doublet and to detect fluorescence of the other "D line" (from the other J state of the doublet) caused by collisions with foreign-gas atoms or the other alkali atoms in the vessel. The collisions with inert gases are "sudden" compared to the ^2P fine-structure separation frequencies for Li and Na, but not for Rb and Cs. This availability of different fine-structure separations and of a variety of inert gases makes this a favorable process for studying the transition from sudden to adiabatic atom-atom collisions.

This paper reports measurements of these Rb–inert-gas and Cs–inert-gas cross sections that have been obtained by a minor extension of standard techniques. We will follow standard procedure and discuss these measurements in terms of a "cross section" $Q(T)$ that is defined in terms of the measured rate of excitation transfer $R(T)$ by $R(T) = \rho\bar{v}\, Q(T)$, where ρ is the foreign-gas density, $\bar{v}$ the mean interatomic velocity, and T the kinetic temperature of the vapors. This "cross section" $Q(T)$ is an average of the actual cross section, which we will call $\sigma(v)$, over the thermal interatomic-velocity distribution $P(v,T)$ of the gases in a vessel.

Since the earliest investigations, values of $Q(T)$ in the neighborhood of 10^{-14} cm^2 for $T \cong 350$°K have been reported for the Na and K doublet transitions caused by inert-gas collisions. But recent work, mostly by Krause and his associates, has shown that the $Q(T)$ $(\cong 350$°K) due to inert-gas collisions are between 10^{-17} cm^2 and 10^{-19} cm^2 for the Rb doublet and between 10^{-19} cm^2 and 10^{-21} cm^2 for the Cs doublet.[1] This drastic reduction in Q is clearly a result of the increased ^2P energy gaps (ΔE) of Rb and Cs, which makes these collisions more nearly adiabatic. The importance of this energy defect in excitation-transfer collisions has been noted,[2] and three different calculations of its effect on these alkali-metal–inert-gas collisions have recently been reported.[3–5]

Without going into a variety of important complications, we can state the fundamental idea by considering a collision in terms of time-dependent perturbation theory. The probability amplitude in the final state at the end of a collision is proportional to a time integral, through the collision, of the perturbation matrix elements times $\exp(i\Delta Et/\hbar)$. If the collision occurs over many cycles of $\Delta E/\hbar$, as with the Rb and Cs doublets, the oscillatory function $\exp(i\Delta E/\hbar)$ will cause a reduction in the transition probability.[6] But for the Na and K doublets, most of the effective 350°K collisions, which have impact parameters below 10 Å, take place within a cycle of ΔE and it has only a minor effect. [It is not obvious just where ΔE becomes a minor factor, but in these cases it would appear to be one, since Callaway and Bauer's calculation[7] for Na and K, in which ΔE is neglected, agrees roughly with experiment. In addition, nonresonant depolarization cross sections are about 10^{-14} cm^2, and these arise from (degenerate) Zeeman-level mixing by the same atom-atom electrostatic interaction potential. Nikitin,[5] however, finds the K cases slightly adiabatic.]

The extent to which a particular doublet-transfer collision is sudden or adiabatic depends, of course, on the interatomic velocity as well as on ΔE. Thus, a rapid variation of $\sigma(v)$ with velocity, as well as with ΔE, is expected. Indeed, this has already been confirmed by the results of Krause and his associates, since their reported Cs and Rb cross sections against He are roughly two orders of magnitude greater than against the heavier (and slower) inert gases. It is also apparent that $\sigma(v)$ must be an extremely rapid function of ΔE and v, since the ΔE of K, Rb, and Cs are 58, 238, and 554 cm^{-1}, respectively, while their Q (350°K) range across many orders of magnitude.

The present investigation has obtained a low resolution measurement of $\sigma(v)$ for the Rb and Cs collisions with inert gases by measuring $Q(T)$ with T varied from 300 to 900°K. By this procedure the thermal interatomic velocity distribution has been scanned across $\sigma(v)$, and the shape of $\sigma(v)$ with 5×10^4 cm/sec $\leq v \leq 5 \times 10^5$ cm/sec could be established from the data. Also, in this manner the variations in the $Q(T)$ due to different inert-gas velocity distributions are necessarily separated from actual variations in $\sigma(v)$ due to different alkali-metal–inert-gas interactions.

The measured $\sigma(v)$ for Rb and Cs follow a general pattern that is similar for all the inert gases. Consequently, the basic form of all the cross sections are consistent with a "universal" $\sigma(v)$ that spans four orders of magnitude for each alkali metal.

DESCRIPTION OF THE EXPERIMENT

A. Method

The basis of the experimental method used here has been thoroughly described by other investigators,[1] but it will be briefly reiterated to fill in details of our techniques. A mixture of Rb (or Cs) with an inert gas is pumped by the alkali $D1$ line, which is filtered from the radiation of a Rb (or Cs) lamp (the $D1$ line refers to the $n^2P_{1/2}$-$n^2S_{1/2}$ radiation, $D2$ to $n^2P_{3/2}$ -$n^2S_{1/2}$). A phototube detects part of the $D1$ fluorescence intensity ($I_{1\to 1}$), then a $D2$ filter is placed between the scattering vessel and the phototube and the same proportion of the $D2$ fluorescence intensity ($I_{1\to 2}$) is detected (see Fig. 1). If the Rb (or Cs) vapor density is small enough to produce a resonance-line optical depth much less than one, the foreign-gas density is small enough to leave $I_{1\to 2}/I_{1\to 1} \ll 1$, and if the phototube has equal quantum efficiency at both lines, then the measured intensity ratio will establish

$$R_{1\to 2}(T)\tau_1 = I_{1\to 2}/[D2 \text{ filter transmission} \times I_{1\to 1}]. \quad (1)$$

Here $R_{1\to 2}(T)$ is the collisionally induced transition rate from state $1(^2P_{1\,2})$ to state $2(^2P_{3/2})$, τ_1 is the radiative lifetime of state 1, and $Q_{1\to 2}(T)$ is defined by $R_{1\to 2}(T) = \rho v Q_{1\to 2}(T)$ with $\bar{v} = (8kT/\pi\mu)^{1/2}$. To measure $Q_{2\to 1}(T)$, 1 and 2 are reversed in the above procedure.

If the D-line optical depths are not negligible, the primary result will be an increase beyond the natural lifetime of the time available for a collision, and therefore an apparent increase in the $Q(T)$. If $R_{2\to 1}(T)\tau_2$ is not much less than 1, some $2\to 1$ back transfer will compete with the $1\to 2$ transfer, and the actual $R_{1\to 2}(T)\tau_1$ will exceed the measured ratio in (1). In the present experiments, the $R_{i\to j}(T)\tau_i$ were kept between 10^{-6} and 10^{-2}, the resonance-line optical depths were always small enough to produce less than 5% increase in the effective τ (usually much less), and the relative quantum efficiency of the S-1 photomultiplier was calibrated[8] and used to express (1) in terms of the anode currents (the index of refractions and reflectivities of the lenses in the detection optics do not change significantly between the $D1$ and $D2$ wavelengths, so the photocathode causes the only significant variation in detection efficiency).

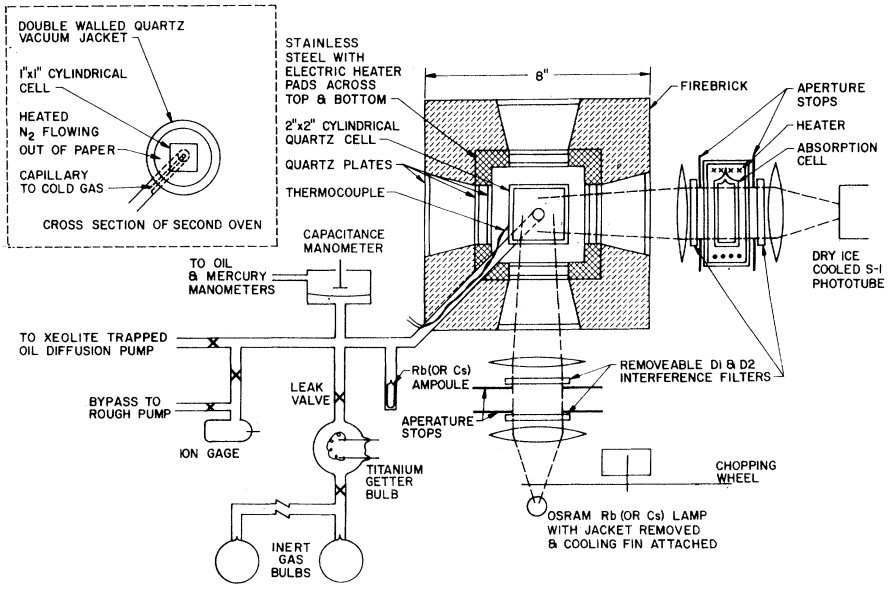

FIG. 1 Optical and vacuum systems. The optical system is drawn roughly to scale. The heaters produced less than 0.5 G of magnetic fields, and the earth's field of about 0.5 G was primarily vertical (out of paper).

The scattering signal versus optical depth was roughly established by measuring the percent absorption of the resonance lamp $D2$ line by the scattering cell vapor. This measurement was made at about 20% absorption, then the data was taken at densities that gave less than $\frac{1}{4}$ as much scattered intensity. Since temperature and line-broadening collisions both effect the optical depth, the $I_{i\to j}/I_{i\to i}$ ratios were taken over a range of presumably insignificant optical depths (scattered light amplitudes) to guarantee that radiation trapping did not influence the cross sections. The linearity of the intensity ratios as a function of inert-gas pressure was also established; the largest densities used were about 200 Torr.

To minimize the oven thermal radiation seen by the phototube, windows were placed in all sides of the oven (see Fig. 1). Nonetheless, some residual black-body radiation was received by the phototube through the ~ 60 Å half widths of the interference filters. Since the Rb and Cs D lines are between 7800 and 8950 Å, this black-body radiation exceeded the $I_{i\to j}$ signals at temperature above roughly 300°C. Light chopping and lock-in detection was used to minimize this source of noise, but it ultimately set a high-temperature limit on the data. (Rb-He data were taken to 1200°K but with inadequate accuracy to establish anything other than an obvious extrapolation of the reported data.) A second oven with all quartz surfaces and hot flowing nitrogen heating was used to improve signal to noise for the Cs data. The thermal properties of these ovens are discussed later.

B. Impurities

The Rb and Cs doublet-transfer cross sections for collisions with polyatomic gases are about 10^{-15} cm^2,[9] because the vibrational-rotational structure of the molecular ground state can generally find a near overlap with ΔE, allowing transfer of energy between internal coordinates rather than into the kinetic energies. The cross sections for the Cs–inert-gas collisions are as low as 10^{-22} cm^2, in which case a polyatomic impurity concentration in the inert gas of one part in 10^7 could overshadow the measured doublet transfer. Consequently, the stainless-steel and glass vacuum system was thoroughly baked out before the Rb (Cs) ampoules were broken and high-purity inert gases (Matheson Research Grade) were further cleaned in a flashed titanium gettering bulb. Even Ne that was assayed as spectroscopically clean to 1:10^6 produced excessive cross sections against Cs if used before allowing a cleaning period in the titanium bulb. An additional cleaning by the Cs appeared as a decrease in cross sections within the first five minutes after introducing titanium-cleaned Ne into the cell.

With the exception of $Q(T)$ near 10^{-22} cm^2, where the signal-to-noise ratio was very poor, an upper limit can be estimated for the residual effects of impurities. Indeed, several arguments assert that they make a negligible contribution to the $Q(T) \geq 10^{-21}$ cm^2, and, at worst, a minor contribution to the smaller $Q(T)$. First, the entire set of $Q(T)$ for each alkali against the various inert gases conform to a consistent pattern, whereas the impurity concentrations of the commercial inert gases are quite varied. Next, the $Q(T)$ from polyatomic impurities will not exhibit the rapid temperature variations of the inert gas $Q(T)$. They would tend to alter the $Q(T)$ data by roughly an additive constant, thereby producing a noticeable distortion in the low-temperature end of the $Q(T)$ curves. Finally, the inert gases and the vacuum system were treated identically for all the data, so any impurity-produced cross section would have to appear in the very small $Q(T)$ data – as indeed did happen. The maximum impurity-produced Q seen in the Cs-Ne data was 5×10^{-22} cm^2 during the first few minutes of Ne on Cs, and this apparently dropped to a value below 5×10^{-23} cm^2, judging by the consistency of the low-temperature Cs-Ne data.

The effect of degassing from the walls of the vacuum system was easily evaluated (and found negligible) by closing the valve to the pump and looking for an increase of $I_{i\to j}/I_{i\to i}$. This intensity ratio is of course nonzero even without collisional transfer due to interference filter leakages. Using double interference filters, this leakage factor was about 10^{-5} for the Rb lines and 10^{-6} for Cs; in neither case did subtracting filter leakage from the measured ratios influence the cross-section accuracy. Rb-Rb or Cs-Cs collisions are a negligible source of transfer at the vapor pressures used (where the data indicated that the optical depth in 2 cm was less than 0.10 in the center of the strongest $D2$ component). The Rb and Cs were high-purity Penn Metals Company ampoules, and each was distilled into the cell (see Fig. 1). Any impurities would have acted as part of those coming from the walls of the vacuum system.

C. Line Broadening

The $Q_{1\to2}(T)/Q_{2\to1}(T)$ ratio must correspond to the detailed-balancing value of $2\exp(-\Delta E/kT)$ regardless of what gas is causing the transfer, so the apparent violation of this ratio reported in Ref. 1 has been an interesting mystery (we refer to the low foreign-gas density measurements, which cannot be influenced by quenching of the P states). We initially measured similarly incorrect ratios in this experiment, but discovered that they are caused by the non-Lorentzian red wing of the collisionally-broadened resonance lines. Specifically, after the vapor absorbs a <0.1 cm^{-1} wide, primarily Doppler-shaped lamp $D2$ line, it radiates a collisionally-broadened $D2$ line (due to the inert-gas collisions). The $D1$ interference filters pass a 60 Å band on the wing of this broadened line, centered on the

$D1$ line, and the intensity thus received by the detector is proportional to the inert-gas pressure, just as the $2 \rightarrow 1$ transfer is. (This linearity was experimentally verified, but it could hardly be otherwise at the experimental pressures of ≤ 200 Torr.) Of course, it is a very small proportion of this broadened $D2$ line that passes through the $D1$ filters, but also only a very small proportion of the excited atoms are collisionally transferred to the $D1$ state.

For the pressures used (≤ 200 Torr) the $2 \rightarrow 1$ transfer process will produce a broadened $D1$ line that nonetheless has 99% of its intensity within 1 cm^{-1}, while the broadened $D2$ line will be spread fairly uniformly across the 60 Å region passed by the $D1$ filters. If a Rb (or Cs) absorption cell, with an optical depth of about 5 at line center and with 100 Torr of argon for broadening is placed between the $D1$ filters, it will absorb virtually all of the $2 \rightarrow 1$ transfer radiation but very little of the broadened $D2$ radiation. In our experiments, the $I_{i \rightarrow j}/I_{i \rightarrow i}$ ratios were measured with and without such an absorption cell between the detector filters (see Fig. 1). It was found that the line broadening contributed to the $I_{2 \rightarrow 1}$ to cause an error in $Q_{2 \rightarrow 1}$, but no such contributions to the $Q_{1 \rightarrow 2}$ were detected. This is consistent with the non-Lorentzian red-shifted line wings that have been predicted and observed.[10-12] This correction to our measured $Q_{2 \rightarrow 1}$ removed all detailed-balancing discrepancies (within the experimental uncertainties, which were generally less than 10%). In the Cs-Ne experiments, the $2 \rightarrow 1$ transfer cross sections were so small that the broadened $D2$ line produced almost all of the crossed fluorescence at the lower temperatures. The necessity of subtracting off this large proportion of the total $2 \rightarrow 1$ crossed fluorescence increased the uncertainties in these Cs-Ne measurements. Nonetheless, it is clear from the data that this phenomenon explains all discrepancies greater than 30% with the results of Krause and his associates for Rb-He, Rb-Ne, and Cs-He cross sections. For the remaining Rb and Cs cross sections, this is not sufficient to explain all the discrepancies, and we suspect that polyatomic impurities in the inert gases also contributed to their cross sections.

A more thorough investigation of the complete line profiles at various temperatures is under way, particularly since this provides considerable information about the shapes of the energy levels of Rb*(or Cs*) inert gas as functions of interatomic position,[12] and a $^2P_{3/2} \rightleftarrows {}^2P_{1/2}$ transfer calculation should utilize this information.

The Rb and Cs line-broadening measurements of Chen and Jefimenko[10,11] show the relative shape of the red wing, but not the size of this wing relative to the total line intensity, so we cannot directly check the intensities we measured against other data. We have found that at fixed inert-gas density the proportion of the broadened $D2$ line passing the $D1$ filters increases with the heavier inert gases. *Also, it increases with decreasing temperatures, with as much as a factor of* 5 *variation between* 900 *and* 300°K. This is primarily due to the temperature dependence of the (collisional) distribution of interatomic positions in the (alkali)*–inert-gas interatomic potential.

D. Nonthermal Velocity Selection

Since these transfer cross sections are very rapidly increasing functions of the collision velocity, any high-velocity selection in the excitation process could distort the data. In particular, if the exciting radiation were badly self-reversed, the higher-velocity Rb (or Cs) atoms would be preferentially excited. Of course only one component of velocity for only one of the colliding particles would be thus selected, but a rough calculation indicates that this could potentially cause 50% errors for the lower-temperature collisions with the heavier inert gases. Consequently in the Rb-Ar experiment, magnetic fields up to 2 kG were applied to the lamp to smear out any such self-reversals. Less than a detectable 2% change in the cross sections was noted under these conditions, so all other data were taken without the fields. The Osram lamps used were operated at 0.7 A of 60-cps power with the jackets removed, and a cooling fin attached at one end for convective air cooling. Under these conditions, they provided about the maximum fluorescence intensity, which was roughly $\frac{1}{4}$ as strong as could be obtained from a 2.4-kMc/sec excited flow lamp the latter was only used for testing .[13]

E. Control of the Alkali Densities

Rubidium and cesium in glass or quartz containers demand special techniques for adjusting their densities, since the surfaces tend to "soak up" large quantities of the alkali and then release them gradually. In these experiments the equilibrium vapor pressures of the cold tube leading to the vacuum system had very little effect on the alkali-metal density in the cell. When an increase in alkali-metal density in the cell was desired, it was achieved either by briefly heating the saturated side tube to drive in some vapor or by heating the cell slightly (the former process is not effective with inert gas also in the tube). When a decrease in density was desired, it was achieved by cooling the cell slightly or by heating it (typically by 200°C for an hour) to drive some of the alkali metal out, then cooling back down. A 10°C change in temperature was sufficient to change the density in the cell by about a factor of 2, starting from any temperature between 0 and 900°C. In this manner the vapor densities in the cell could be maintained for hours at any desired level, which was generally far below that corresponding to room temperature equilibrium. Since it took much longer to drive the alkali metal out rather than in, most of the data was taken starting with an appropriate density at high temperature, then continually lowering the temperatures and driving in more alkali metal when needed.

Although Na and K are known to react with Pyrex and quartz, no discoloration of the quartz cell was observed at the end of months of operation,

often for weeks at elevated temperatures, in contact with Rb and Cs vapor.

F. Zeeman Transitions

These $^2P_{1/2} \rightleftarrows {}^2P_{3/2}$ transfer cross sections are much smaller than the $^2P_{3/2}$ state depolarization cross sections of about 10^{-14} cm^2. Since all data other than Rb-He was taken with inert-gas pressures greater than 10 Torr, any $^2P_{3/2}$ state alignment along the exciting beam axis would have been almost completely destroyed by collisions during the excited state lifetime. Since we excited with and detected unpolarized radiation, only alignment could contribute to the observed intensities. Thus the radiation from either J state was isotropic and unpolarized regardless of possible differences between $J,m \rightleftarrows J',m'$ cross sections. In the case of Rb-He a few percent anisotropy might be possible in the $^2P_{3/2}$ decay, but no more than this because the anisotropy even without collisions is only in the neighborhood of 10%due to the hyperfine structure. Thus our experimental $J \rightleftarrows J'$ cross sections are an average over all the individual Zeeman transitions.

The inert-gas pressures (between 0.1 and 200 Torr) were measured using a capacitance manometer as a null device to isolate the clean system from oil and mercury manometers. The approximately 2% uncertainty in these pressures is a negligible source of error in the experiment.

Since the cross sections varied typically as $T^{2.5}$, a 4% error in absolute temperature is equivalent to a 10% error in cross section. In the stainless-steel oven one thermocouple was kept in contact with the inside of the stainless-steel wall and another with the cell wall. The one against the stainless-steel registered about 4% higher temperatures (above room temperature). The temperatures of the cell wall thermocouple were used in the data plots, but with some trepidation since this Chromel-Alumel thermocouple had a much greater emissivity than the cell walls, and the oven windows subtend about 15% of the total solid angle from this point; i. e., the thermocouple is not in an isothermal cavity and gas conduction must compete with radiation losses. Thus, even though the two thermocouples gave a fairly constant temperature ratio, one might suspect that at the higher temperatures the inner thermocouple was a few percent too cool. A temperature uncertainty in the other direction was indicated by the fact that the alkali-metal vapor pressure and the transfer cross sections, which were very sensitive to the inner cell wall temperature, lagged the thermocouple by 5 to 20 min. Also, the transfer cross sections and alkali vapor density would slowly decrease (typically by 10%) after introducing the inert gas, without a corresponding change in the thermocouple reading. (This does not appear to be cooling by convection out the 6-mm transfer tube.) Altogether, the uncertainty in $T-300$°K appears to be about ±5%.

In the hot-gas heated oven used for the Cs-Ne data, the temperature uncertainty was greater yet. Here a double-walled quartz vacuum jacket was the only oven wall, so Pt-Rd thermocouples were used for their lower emissivity. Thermocouples placed on sides of the cell towards and away from the hot-gas source registered 15% variation in $T-300$°K. Amazingly enough, Cs-He data taken with this oven, using the averaged thermocouple readings, agreed within experimental scatter with data from the stainless oven (see Fig. 2). Nonetheless, 5% uncertainty in $T-300$°K is probably somewhat optimistic for this data.

The accuracies in cross-section measurements were better for Rb than Cs since the Rb D lines are separated by only 150 Å, compared to 430 Å for Cs, and the Rb cross sections are much larger. The phototube quantum efficiency varies only a few percent between the Rb D lines, but nearly 10% for the Cs lines. Although the relative quantum efficiency of the phototube was calibrated in both cases, and the lens indices of refraction do not change significantly between either set of D lines, this does not prevent several percent added uncertainty in the Cs case. Another problem is the angular dependence of the interference filter transmissions. The filter transmissions of the fluoresced D lines were calibrated with the filters in position between scattering cell and photomultiplier, but not without a few percent uncertainty. The sensitivity of the phototube and lock-in detector across the 10^5 experimental range of intensities were measured, but again to no closer than a few percent. Phototube shot noise was not a problem for any cross sections above 10^{-20} cm^2, but it caused as much as 30% of scatter in the 3×10^{-22} cm^2 cross sections.

The line-broadening feedthrough signals were much smaller than the $2 \rightarrow 1$ transfer signal for Rb-He, Ne, Ar, and for Cs-He. But in the low-temperature Rb-Kr, Xe, and Cs-Ne collisions most of the total $2 \rightarrow 1$ signal was from line broadening. The desired $2 \rightarrow 1$ signal was the residue left after correcting the line-broadening signal for absorption-cell window attenuation, then subtracting this and filter leakages from the total $2 \rightarrow 1$ signal. The wall scattering of the absorption cell was calibrated with tungsten radiation filtered by the D-line interference filters, and its absorption of the actual D-line fluorescence was calibrated using the actual $2 \rightarrow 2$ and $1 \rightarrow 1$ broadened fluorescence. But several more percent of error were rapidly accumulated in this manner, particularly when the $2 \rightarrow 1$ collisional transfer signal was only a small part of the total $2 \rightarrow 1$ signal.

Finally, the possibility of polyatomic impurities causing increases in the measured cross sections has already been noted. The systematic behavior of the data tends to discount this possibility, but it is unlikely that additions of several percent at the lower temperatures would be apparent.

In conclusion, the Rb cross sections are assigned about ±15% accuracy, as are the Cs-He cross sections. But the Cs-Ne cross-section uncertainties should be about 20% at 10^{-20} cm^2, increasing to perhaps ±40% at 10^{-22} cm^2. With

the exceptions of Cs-Ne, we consider these to be about 90% confidence limits, well in excess of measured fluctuations.

RESULTS

The $Q(T)$ data are plotted against

$$T' = T \times (\mu_{\text{alkali-He}}/\mu_{\text{alkali-inert-gas}})$$

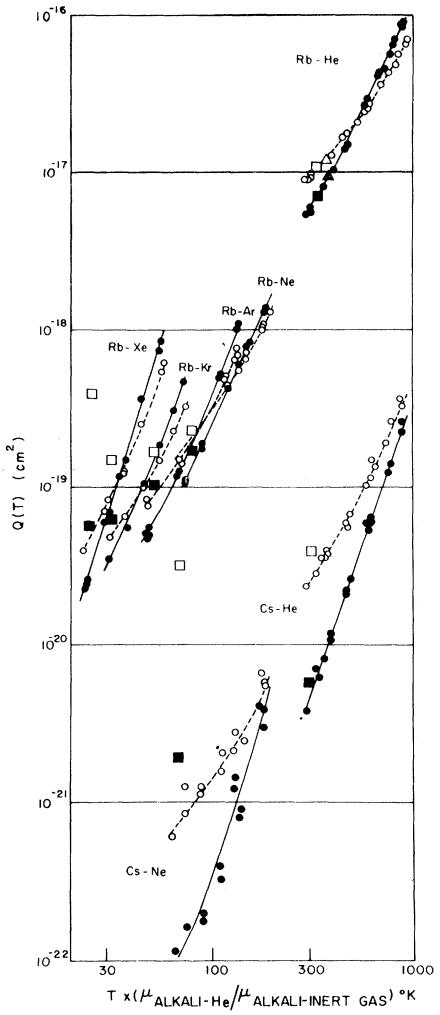

FIG. 2. The measured doublet-transfer "cross sections" $Q(T)$. The $Q(T)$ are plotted as a function of a reduced temperature which describes the distribution of collision velocities. The $^2P_{3/2} \rightarrow {}^2P_{1/2} Q(T)$ are dashed lines and open-circle data points. The $^2P_{1/2} \rightarrow {}^2P_{3/2} Q(T)$ are solid lines and solid data points. In the Rb-Ar and Rb-Ne overlap region the data points are omitted to prevent confusion.

The measurements of Krause's group[1] are indicated as □ for $^2P_{3/2} \rightarrow {}^2P_{1/2}$ and ■ for $^2P_{1/2} \rightarrow {}^2P_{3/2}$. The Rb-He results of Ref. 14 are respectively △ and ▲. The Cs-He data were taken in two oven and cell arrangements, but any differences were no greater than the scatter, and both sets of data are plotted here. The ratios of $^2P_{1/2} \rightarrow {}^2P_{3/2}$ to $^2P_{3/2} \rightarrow {}^2P_{1/2}$ "cross sections" correspond to the detailed balancing ratio $2\exp(-\Delta E/kT)$.

in Fig. 2. In this manner the data are plotted at the temperature T' for which the alkali-helium velocity distribution $P(v, T')$ equals the actual $P(v, T)$, giving a plot of all the "cross sections" versus alkali-helium velocity distribution. This corrects for the differences between $Q(T)$ that are caused by the different μ in the Maxwellian velocity distributions. Thus the differences in Fig. 2 between the Rb-Ar and Rb-Kr "cross sections" at $T' = 70°$K must arise from different interactions, because the distributions of collision velocities are the same. It can be seen from Fig. 2 that the Rb-He (Cs-He) $Q(T)$ are fairly close to an extrapolation of the Rb-Ne (Cs-Ne) $Q(T)$ to higher temperatures. From the discussion of Fig. 3 that follows, it will be clear that this results from a common $\sigma(v)$ behavior. The actual data

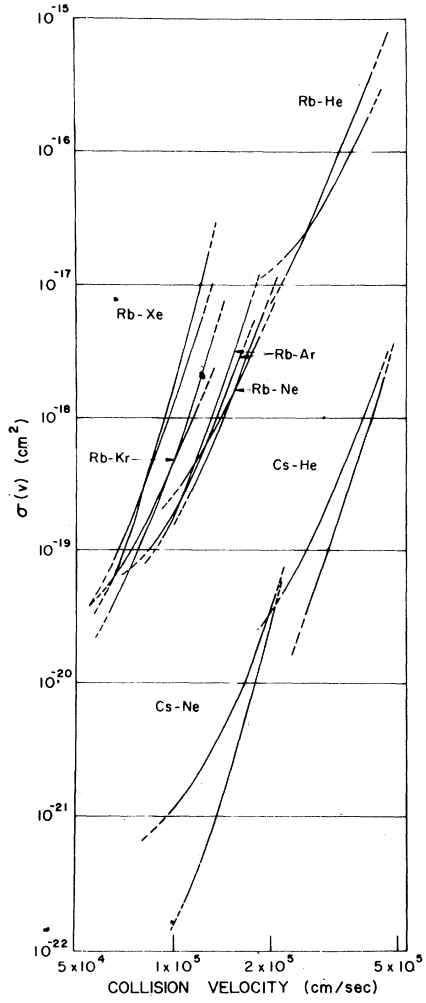

FIG. 3. The "average" $\sigma(v)$ cross sections, as deduced from the $Q(T)$ data. These are plotted as solid lines between the velocities v_m at which the largest contributions to $Q(900°\text{K})$ and $Q(300°\text{K})$ occur. They have been extended as dashed lines $0.1\, v_m$ to either side, since these regions also contribute significantly to the measured $Q(T)$. The $^2P_{3/2} \rightarrow {}^2P_{1/2}$ and $^2P_{1/2} \rightarrow {}^2P_{3/2}$ cross sections have not been distinguished since the assignment is apparent from Fig. 2.

were taken at 300–900°K in each case, and can be immediately obtained by the appropriate horizontal displacements on the log-log plot of Fig. 2. Data taken above 900°K were less accurate because of background oven radiation and temperature uncertainties, so they have not been included. The best data above 900°K were on Rb-He from 900–1200°K. Within the increased experimental error of perhaps ±25% these data fit the obvious extrapolation of the plotted Rb-He data.

The experiments were not continued to Cs-Ar, -Kr, or -Xe, because of the time necessary to eliminate impurity contributions and increasing line-broadening contributions in the presence of barely adequate 5-min signal-to-noise ratios.

The $Q(T)$ come from the velocity integral of $v\sigma(v)P(v,T)$, as expressed in Eq. (3). By varying the temperature we have scanned $P(v,T)$ across the various $v\sigma(v)$, but $P(v,T)$ covers a considerable range of velocities and this process certainly has not uniquely established $\sigma(v)$. However, we can use the $Q(T)$ data to establish an average $\sigma(v)$, which must agree with an average across a fairly small velocity range of the true $\sigma(v)$. We proceed as follows.

From the Maxwellian velocity distribution

$$P(v,T) = 4\pi^{-1/2}(\mu/2kT)^{3/2}v^2\exp(-\mu v^2/2kT), \quad (2)$$

and

$$Q(T) = \int_0^\infty \sigma(v)P(v,T)vdv \Big/ \int_0^\infty P(v,T)vdv, \quad (3)$$

it follows that $\sigma(v) = Kv^{2n}$ produces a $Q(T) = K\Gamma(n+2)(2kT/\mu)^n$. It appears that the converse must also hold: a $Q(T)\propto T^n$ must be caused by a $\sigma(v)\propto v^{2n}$ for all velocities that contribute significantly to the first integral in (3). On the other hand, the $\sigma(v)$ across a range of velocities contribute to each $Q(T)$, so a $\sigma(v)$ proportional to v^{2m} would on the average, but with additional rapid fluctuations in $\sigma(v)/v^{2m}$, produce a $Q(T)$ which barely indicated the presence of the rapid fluctuation. The fact that the data in Fig. 2 fit curved lines, rather than straight lines corresponding to T^n, presents little difficulty, because each measured $Q(T)$ can be quite accurately fitted to the sum of two straight lines. But it is more difficult to put a limit on what sort of rapid fluctuations in $\sigma(v)$ might have been missed due to the typically 10% uncertainty in $Q(T)$ measurements. (We feel, on theoretical grounds, that $\sigma(v)$ fluctuations sufficiently rapid to escape detection in these experiments are very unlikely.) This fluctuation problem and the identification of what velocity regions contributed to each $Q(T)$ will now be considered.

The slopes of the $Q(T)$ lines in Fig. 2 correspond to $Q(T)\propto T^2$ to $T^{4.5}$, and they vary rather slowly with temperature (in the worst cases they change a factor of 2 for a factor of 3 temperature change). Since these slopes change gradually, we can take as a first approximation that each $Q(T)\propto T^n$ region is produced by a $\sigma(v)\propto T^{2n}$ in the appropriate velocity region. Here we are neglecting possible rapid fluctuations about the average shape as well as "curvature" in $\sigma(v)$, but the essential point is that the data correspond to $\sigma(v)$ whose average velocity dependences are between v^4 and v^9. The integrand of Eq. (3), $P(v,T)v\sigma(v)$, has been normalized at its maximum value and plotted in Fig. 4 for a $\sigma(v)\propto v^4$ and a $\sigma(v)\propto v^8$. The normalization constants and the areas under these curves determine the $Q(T)$, and their most significant feature is the comparatively small range of velocities which contribute the major part of these areas.

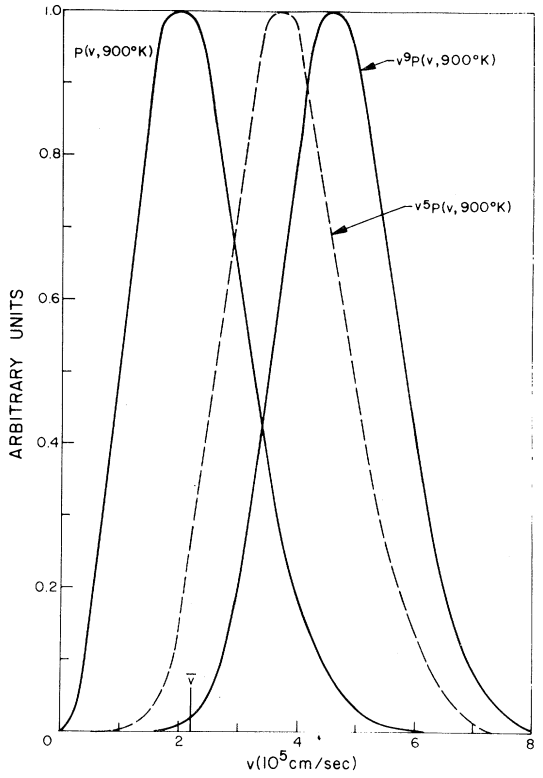

FIG. 4. $P(v,T)$ and $P(v,T)\,v\sigma(v)$ for Rb-He at $T = 900°$K. Two cases are shown, $\sigma(v) \propto v^4$ and $\sigma(v) \propto v^8$. Each of the functions is normalized to produce a peak height of 1.0. Varying T changes only the velocity scale.

Calling the velocity at the peak v_m, one half of the area comes from a velocity range $v_m(1\pm 0.18)$ for $\sigma(v)\propto v^4$ and $v_m(1\pm 0.14)$ for $\sigma(v)\propto v^8$. Changing T from the 900°K example merely changes the velocity scale of Fig. 4, so it appears that the $Q(T)$ come from integrations that heavily weight a 30–40% range of velocity. We can use this to put a rough limit on the kind of rapid fluctuations in $\sigma(v)$ that might have been missed. If we represent the possibility of such structure by $\sigma(v) = cv^n f(v)$, with $f(v) = 1$ on the average, then the $Pv\sigma$ plots in Fig. 4 would be multiplied by $f(v)$. It appears unlikely that the experimental $Q(T)$ resolution of typically 5–10% was sufficient to detect any $f(v)$ that varied by x% across less than ~ $(600/x)$% range in velocity. In a nutshell, we did not expect such variations, so we did not complicate the experiment by looking for them. About a 1% relative accuracy in the Rb $Q(T)$ could probably be achieved.

Another interesting feature in Fig. 4 is the velocity region which contributes to the $Q(T)$ integral. In the $\sigma(v) \propto v^8$ case this region is centered on 2.08 $\bar{v}$, at which velocity $P(v, T)$ is only 7% of its maximum value but $\sigma(v)$ is 350 times $\sigma(\bar{v})$. It is apparent that the high-velocity tail of $P(v, T)$ is producing the $Q(T)$ in these experiments; and that as the $Q(T)$ slopes in Fig. 2 increase, the effective area of the $P(v, T)$ tail decreases. Consequently the $\sigma(v)$ which produce each $Q(T)$ greatly exceed this $Q(T)$.

Most of the $Q(T)$ data in Fig. 2 does not fit straight lines, but the curvature in the smooth lines drawn through the data is small enough to allow an accurate matching with the sum of two straight lines (within the 300–900°K range of the data). Consequently, for reducing the $Q(T)$ data to $\sigma(v)$ information, we have used the convenient simplification of matching each $Q(T)$ to

$$Q(T) = \sum_{i=1}^{2} K_i \Gamma(n_i + 2)(2kT/\mu v_0^2)^{n_i}, \qquad (4)$$

where $v_0 = 10^5$ cm/sec. (This method of fitting the data should not be taken to imply that the data corresponds to power law $\sigma(v)$; many different functions can be fitted over a limited range in this manner.) From the above arguments and the linear relationship between Q and σ, it then follows that such a $Q(T)$ would be produced by an "average" $\sigma(v)$ which equalled

$$\sum_{i=1}^{2} K_i (v/v_0)^{2n_i}$$

across the appropriate range of velocities. [To facilitate evaluation of these results, we have included a table of the constants K_i and n_i (see Table I).] For this $\sigma(v)$ the maximum of $P(v, T)$ $v\sigma(v)$ occurs at

$$\frac{v_m}{v_0} = \left[\left(\frac{n_1 K_1 (v_m/v_0)^{2n_1} + n_2 K_2 (v_m/v_0)^{2n_2}}{K_1 (v_m/v_0)^{2n_1} + K_2 (v_m/v_0)^{2n_2}} + \frac{3}{2} \right) \frac{4kT}{v_0^2} \right]^{1/2},$$

a number that is easily evaluated by graphing or by successive approximations. In Fig. 3 the various "average" $\sigma(v)$ are plotted as solid lines between the v_m of 300 and 900°K, and as dashed lines for another $0.1 v_m$ either side of this.

The accuracy of the $Q(T)$ was estimated at about ±15%, except for Cs-Ne which was more like ±40%. The measurements of the temperature-dependent variations in each $Q(T)$ were more accurate, but a 5% uncertainty in $T - 300$°K also existed. These uncertainties of course extend over into the $\sigma(v)$, giving an estimated 10% uncertainty in the slopes of the lines and 15% uncertainty in any specific $\sigma(v)$; about 20 and 40% for Cs-Ne. In addition, the extreme values of $\sigma(v)$ are not as well determined by the limited $Q(T)$ scan, causing about 10% additional uncertainty at the limits plotted. Aside from these uncertainties, we do not see how any other set of "average" $\sigma(v)$ could possibly produce the $Q(T)$ data, and it even appears very unlikely that the actual $\sigma(v)$should differ from these "average" $\sigma(v)$. Thus the $\sigma(v)$ give a good indication of what a theory must predict, but it is clearly preferable to calculate $Q(T)$ from any theoretical $\sigma(v)$ and compare $Q(T)$ directly to the experimental $Q(T)$.

TABLE I. Constants used to fit Eq. (4) to the $Q(T)$ data.

Cross Section	$10^{20}K_1$ (cm^2)	$10^{20}K_2$ (cm^2)	n_1	n_2
Rb-He $^2P_{3/2} \rightarrow {}^2P_{1/2}$	3.4	490	3.00	0.50
Rb-He $^2P_{3/2} \leftarrow {}^2P_{1/2}$	6.2	220	3.00	0.00
Rb-Ne $^2P_{3/2} \rightarrow {}^2P_{1/2}$	13	13.5	2.64	0.50
Rb-Ne $^2P_{3/2} \leftarrow {}^2P_{1/2}$	15.8	0.0	2.75	–
Rb-Ar $^2P_{3/2} \rightarrow {}^2P_{1/2}$	11.7	6.9	3.10	0.35
Rb-Ar $^2P_{3/2} \leftarrow {}^2P_{1/2}$	11.2	6.7	3.59	1.00
Rb-Kr $^2P_{3/2} \rightarrow {}^2P_{1/2}$	45	1.3	2.62	0.00
Rb-Kr $^2P_{3/2} \leftarrow {}^2P_{1/2}$	51	2.6	3.44	0.50
Rb-Xe $^2P_{3/2} \rightarrow {}^2P_{1/2}$	144	1.6	3.45	0.00
Rb-Xe $^2P_{3/2} \leftarrow {}^2P_{1/2}$	200	0.3	4.17	0.00
Cs-He $^2P_{3/2} \rightarrow {}^2P_{1/2}$	0.0114	0.62	3.24	1.00
Cs-He $^2P_{3/2} \leftarrow {}^2P_{1/2}$	0.0025	0.0	3.70	–
Cs-Ne $^2P_{3/2} \rightarrow {}^2P_{1/2}$	0.048	0.074	2.70	0.80
Cs-Ne $^2P_{3/2} \leftarrow {}^2P_{1/2}$	0.00337	0.0135	4.54	1.9

CONCLUSIONS

The results in Figs. 3 and 4 trace the behavior of an inelastic, atom-atom collision cross section, starting about one order of magnitude below typical cross sections for "sudden" collisions and extending about 10^6 below this. The variations between these cross sections for the different alkali inert-gas combinations are not as striking as their similarity and their rapid variation with v and ΔE.

It has long been recognized and verified[2] that excitation transfer between different species as well as within one atom depends strongly on the velocities and energy gaps. Heavy-particle, high-energy collision cross sections also depend on the competition between collision times and internal energy differences, but in a regime where the interaction energies are large compared to atomic energies and the highly perturbed electronic wave functions are difficult to evaluate. The doublet-transfer cross section studied here is instead characterized by small perturbations of the wave functions and level structure. It would appear to offer a good testing ground for nearly adiabatic collision theories.

*This work was supported in part under National Science Foundation Grant No. GP 6595.

†Of the University of Colorado and the National Bureau of Standards, Boulder, Colorado.

[1]L. Krause, Appl. Opt. 5, 1375 (1966). This article describes the technique and thoroughly references other measurements.

[2]N. F. Mott and H. S. W. Massy, *The Theory of Atomic Collisions* (Oxford University Press, London, 1965), p. 645–654.

[3]P. L. Bender, D. R. Crosley, D. R. Palmer, and R. N. Zare, *Abstracts of the International Conference on the Physics of Electronic and Atomic Collisions*, Leningrad, July 17–23, 1967 (Nauka, Leningrad, 1967), p. 510.

[4]E. I. Dasheriskaya and E. E. Nikitin, Opt. i Spektroskopiya 22, 866 (1967) [English transl: Opt. Spectry. (U.S.S.R.) 22, 473 (1967)].

[5]H. I. Mandelberg, private communication. Submitted to the "Conference on Heavy Particle Collisions," Belfast, Ireland, April 1–3, 1968.

[6]This oversimplification neglects a variety of features, such as the dependence of ΔE and the mixing interaction on internuclear separation.

[7]Joseph Callaway and Ernest Bauer, Phys. Rev. 140, A1072 (1965).

[8]Alan Gallagher, Phys. Rev. 157, 24 (1967). The calibration procedure is described here.

[9]D. A. McGillis and L. Krause, Phys. Rev. 153, 44 (1967).

[10]Shang-Yi Ch'en, Robert B. Bennett, and Oleg Jefimenko, J. Opt. Soc. Am. 46, 182 (1956).

[11]Oleg Jefimenko and Shang-Yi Ch'en, J. Chem. Phys. 26, 913 (1957).

[12]T. Holstein, Phys. Rev. 79, 744 (1950).

[13]B. Budick, R. Novick and A. Lurio, Appl. Opt. 4, 229 (1965).

[14]T. J. Beahn, W. J. Condell, and H. I. Mandelberg, Phys. Rev. 141, 83 (1966).

Estimation of the Cross Sections for Collision Transfer of Excitation in Helium*

F. T. Chan
Laboratory of Plasma Studies
Cornell University, Ithaca, New York
(Received 6 March 1968)

The Stueckelberg formula is used to estimate the cross sections for the collision transfer of excitation of helium atoms: $He(1^1S_0) + He(4^3P) \rightarrow He(1^1S_0) + He(4^3S) \pm \Delta E$ and $He(1^1S_0) + He(4^3P) \rightarrow He(1^1S_0) + He(4^3D) \pm \Delta E'$. At $T = 600°K$, the calculated cross sections are $Q_{4P\text{-}4S}{}^{tr} = 0.93 \times 10^{-15}$ cm^2 and $Q_{4P\text{-}4D}{}^{tr} = 2.25 \times 10^{-15}$ cm^2, as compared to the experimental values $(0.35 + 0.03) \times 10^{-15}$ cm^2 and $(0.99 + 0.24) \times 10^{-15}$ cm^2, respectively.

Using a helium laser to perturb selected excited-state populations in an auxiliary cell containing a pure-helium-gas discharge at 600°K, Abrams and Wolga[1] recently successfully measured the cross sections for the following collision processes:

$$He(1^1S_0) + He(4^3P) \rightarrow He(1^1S_0) + He(4^3S) \pm \Delta E \quad (1)$$

$$He(1^1S_0) + He(4^3P) \rightarrow He(1^1S_0) + He(4^3D) \pm \Delta E' \quad (2)$$

with the results

$$q_{4^3P\text{-}4^3S} = (0.35 \pm 0.03) \times 10^{-15} \text{ cm}^2 \quad (3)$$

and

$$q_{4^3P\text{-}4^3D} = (0.99 \pm 0.24) \times 10^{-15} \text{ cm}^2, \quad (4)$$

respectively.